The following resources related to this article are available online at www.sciencemag.org (this information is current as of March 12, 2010):

Updated information and services, including high-resolution figures, can be found in the online version of this article at:
http://www.sciencemag.org/cgi/content/full/327/5971/1380

Supporting Online Material can be found at:
http://www.sciencemag.org/cgi/content/full/327/5971/1380/DC1

A list of selected additional articles on the Science Web sites **related to this article** can be found at:
http://www.sciencemag.org/cgi/content/full/327/5971/1380#related-content

This article **cites 37 articles**, 17 of which can be accessed for free:
http://www.sciencemag.org/cgi/content/full/327/5971/1380#otherarticles

This article has been **cited by** 1 articles hosted by HighWire Press; see:
http://www.sciencemag.org/cgi/content/full/327/5971/1380#otherarticles

This article appears in the following **subject collections**:
Biochemistry
http://www.sciencemag.org/cgi/collection/biochem

Restriction of Receptor Movement Alters Cellular Response: Physical Force Sensing by EphA2

Khalid Salaita,[1,2,3]*† Pradeep M. Nair,[1,2,3]* Rebecca S. Petit,[1,2,3] Richard M. Neve,[4]‡ Debopriya Das,[4] Joe W. Gray,[4,5] Jay T. Groves[1,2,3,6]§

Activation of the EphA2 receptor tyrosine kinase by ephrin-A1 ligands presented on apposed cell surfaces plays important roles in development and exhibits poorly understood functional alterations in cancer. We reconstituted this intermembrane signaling geometry between live EphA2-expressing human breast cancer cells and supported membranes displaying laterally mobile ephrin-A1. Receptor-ligand binding, clustering, and subsequent lateral transport within this junction were observed. EphA2 transport can be blocked by physical barriers nanofabricated onto the underlying substrate. This physical reorganization of EphA2 alters the cellular response to ephrin-A1, as observed by changes in cytoskeleton morphology and recruitment of a disintegrin and metalloprotease 10. Quantitative analysis of receptor-ligand spatial organization across a library of 26 mammary epithelial cell lines reveals characteristic differences that strongly correlate with invasion potential. These observations reveal a mechanism for spatio-mechanical regulation of EphA2 signaling pathways.

Mammalian cells exhibit marked sensitivity to physical aspects of their environment, such as compliance (1), texture (2), and geometry (3). Tensional homeostasis between and within cells contributes to proper cell differentiation, development, and, ultimately, survival (4). Because most cellular decision making occurs via chemical processes, understanding the coupling between physical forces and chemical signaling networks is of fundamental importance. Focal adhesions, which consist of protein assemblies organized at sites where cell-surface integrin receptors bind extracellular matrix ligands, are the most widely studied interface for tensile force transduction (5). However, the majority of membrane receptors are not associated with focal adhesions. The mechanisms (and even existence) of chemomechanical regulatory coupling in these systems remain largely unknown.

It is becoming clear that spatial organization of cell surface receptors can regulate associated signal transduction pathways (6–9). An important corollary is that mechanical forces acting on ligands can influence receptor spatial organization and, correspondingly, signaling (10–12).

Juxtacrine signaling, in which receptor and ligand reside in apposed cell membranes, represents an important class of intercellular communication where physical restriction of ligand spatial organization and movement is evident (6, 13). Here, we reconstitute the juxtacrine signaling geometry between live cells expressing the EphA2 receptor tyrosine kinase and supported membranes displaying laterally mobile ephrin-A1 ligand.

EphA2 is implicated and functionally altered in a number of cancers. In particular, 40% of human breast cancers overexpress the receptor (14). Upon binding to natively membrane-anchored ephrin-A1, EphA2 undergoes dimerization, transphosphorylation of the cytoplasmic domains, recruitment of a molecular complex with SHC and GRB2 adaptor proteins, and subsequent activation (15). EphA2 activation stimulates the mitogen-activated protein kinase (MAPK) and the phosphoinositide 3-kinase pathways and recruits the c-Cbl adaptor protein and a disintegrin and metalloprotease 10 (ADAM10), both of which regulate receptor degradation (16, 17). Freely soluble ephrin-A1 ligand binds to EphA2 but fails to trigger activation unless the ligand is chemically cross-linked (18). Despite this observation, most biological and biochemical studies of EphA2 stimulation rely on soluble variants of the ligand (14). We employ a supported-membrane presentation of ephrin-A1 (Fig. 1) that reveals effects of the intrinsic intermembrane physiology on the EphA2 signaling system. This presentation system allows for precise control of membrane chemical composition and lateral organization. Molecules within the supported membrane can be confined within nanoscale corrals by physical barriers to lateral mobility that are prefabricated onto the underlying substrate (7). In the present study, the barriers restrict ephrin-A1 transport (and, thus, EphA2 transport in the live cell) in precisely defined ways. We refer to this type of manipulation as a spatial mutation (7, 19); it generates chemically identical cells that differ only by the spatial configuration of molecules within the specific signal transduction pathway under study.

A fluid supported membrane doped with 0.1% biotin-functionalized lipid was used to generate synthetic cell surfaces presenting laterally mobile ephrin-A1 (Fig. 1 and fig. S1) (20–22).

[1]Howard Hughes Medical Institute, Department of Chemistry, University of California, Berkeley, CA 94720, USA. [2]Physical Biosciences Division, Lawrence Berkeley National Laboratory, Berkeley, CA 94720, USA. [3]Materials Sciences Division, Lawrence Berkeley National Laboratory, Berkeley, CA 94720, USA. [4]Life Sciences Division, Lawrence Berkeley National Laboratory, Berkeley, CA 94720, USA. [5]Department of Laboratory Medicine and Radiation Oncology, University of California, San Francisco, CA 94143, USA. [6]Research Center of Excellence in Mechanobiology, National University of Singapore, Singapore 117543.

*These authors contributed equally to this work.
†Present address: Department of Chemistry, Emory University, 1515 Dickey Drive, Atlanta, GA 30322, USA.
‡Present address: Genentech, 1 DNA Way, South San Francisco, CA 94080, USA.
§To whom correspondence should be addressed. E-mail: jtgroves@lbl.gov

Fig. 1. Scheme of the experimental platform used to trigger and manipulate the EphA2 receptor on the surface of living cells. EphA2-expressing mammary epithelial cells are cultured onto a supported membrane displaying laterally mobile, fluorescently labeled ephrin-A1 ligand. Receptors engage ligands, form clusters that coalesce, and are transported to the center of the cell–supported membrane junction. Nanofabricated chromium metal lines 10 nm in height and 100 nm in linewidth (left cell) act as diffusion barriers and impede the transport of receptor-ligand complexes, leading to an accumulation of Eph-ephrin clusters at boundaries.
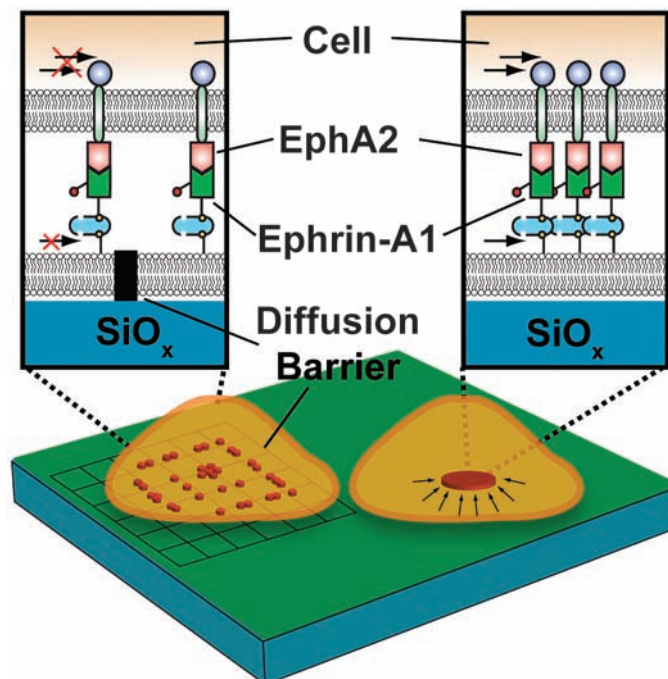
The ligand density on the membrane surface was adjusted to 800 ± 200 molecules/μm^2 (fig. S2) (23), which is comparable to the density of EphA2 receptors on the surface of a representative invasive breast cancer cell line, MDA-MB-231 (fig. S3). When these cells contact functionalized supported membranes, ephrin-A1 becomes organized into microclusters over the course of 15 min (Fig. 2, A and B). Dimerization and oligomerization of Eph receptors upon ligand stimulation is well-documented (24, 25), and higher-order clusters, such as those we observe, have been proposed to exist on the basis of crystallographic studies of the molecular interface in Eph-ephrin complexes (25, 26).

We additionally observe the microclusters to undergo inward radial transport while still bound to the supported membrane, as confirmed by live-cell fluorescence imaging and reflection interference contrast microscopy (RICM), which reveals cell-substrate contact distances (fig. S4 and movie S1) (27). Radial transport characteristics can be quantified for a population of cells by averaging the radial distribution of ligand underneath each cell at defined time points (Fig.

2B and fig. S5). Two-color total internal reflection fluorescence microscopy (TIRFM) tracking of ephrin-A1 and enhanced green fluorescent protein (EGFP) β-actin reveals substantial co-movement between image pairs, suggesting association of the actin cytoskeleton with EphA2 clusters (fig. S6) (22). Further experiments with a Rho kinase inhibitor (detailed below) confirm that EphA2 transport is driven by actomyosin contractility.

The eight different EphA receptors and the five ephrin-A ligands are known to display some promiscuous interactions, but control experiments indicate that ephrin-A1 specifically binds EphA2 (15). First, the EphA2 receptor was highly colocalized with ephrin-A1 (fig. S7A). Additionally, when cells were pretreated with EphA2 antibodies that block the binding site for ephrin-A1, no ligand clustering or cell-surface adhesion was observed (fig. S7B). Large-scale clustering of EphA2 in live cell junctions was also observed when cells that express ephrin-A1 (ZR-75-1) and cells that express EphA2 (MDA-MB-231) were brought into contact for 30 minutes. Immunostaining of cellular junctions with antibodies

specific to either ephrin-A1 or EphA2 indicated accumulation at the contact zone between cells displaying cognate receptor-ligand pairs. Such accumulations resemble those observed in cell–supported membrane experiments (Fig. 2A and fig. S8). Radial transport of receptor-ligand complex was not observed when ephrin-A1–expressing cells contacted EphA2-functionalized supported membranes (fig. S9); thus, receptor translocation is ligand-induced and driven only by the EphA2-expressing cells.

In the preceding experiments, Eph-ephrin binding provided the only physical link between the cell and the supported membrane. RICM confirmed that EphA2–ephrin-A1 clusters colocalize with the regions of closest intermembrane contact (Fig. 2C). To determine if the observed inward radial transport may be an indirect consequence of intermembrane anchoring, a cyclic RGD (Arg-Gly-Asp) peptide-lipid conjugate was included in the supported membrane (22). This peptide serves as a binding partner for integrins on the cell surface (28) and was presented as a binary mixture with ephrin-A1 on the supported membrane in varying densities. RICM images
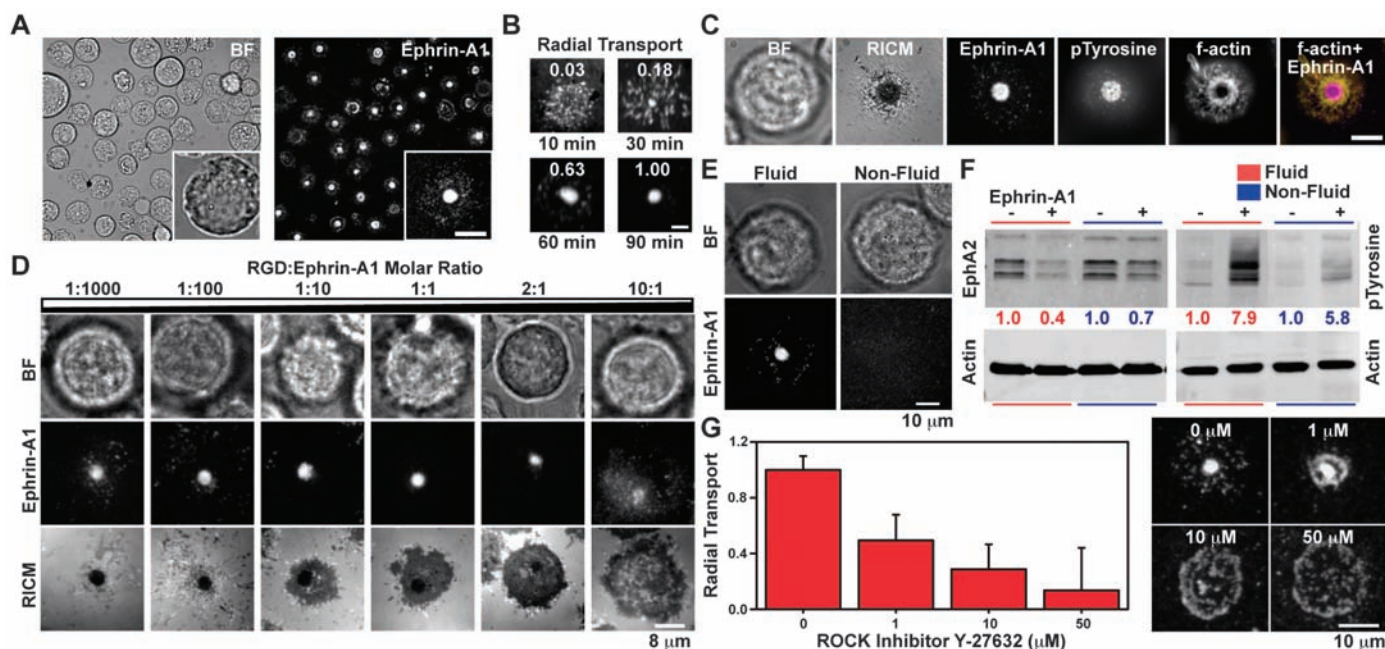

Fig. 2. Mechanical reorganization of ligand-stimulated EphA2. (**A**) Representative bright field and epifluorescence images of MDA-MB-231 cells within 1 hour of interaction with an Alexa Fluor 647–tagged ephrin-A1–functionalized supported membrane. (**B**) Dynamics of receptor-ligand reorganization as a function of time. The radial distribution of ephrin-A1 was measured under each cell, and the population average value ($n = 77$ cells) is indicated above the fluorescence image for each time point. (**C**) The central EphA2 cluster is the region of highest ephrin-A1 concentration, greatest tyrosine phosphorylation, and tightest cell adhesion to the substrate and results in reorganization of the actin cytoskeleton to form a peripheral annulus. Scale bar is 5 μm in (A) to (C). (**D**) Representative bright field, epifluorescence, and RICM images of cells 1 hour after plating on a supported membrane functionalized with binary mixtures of ephrin-A1 and cyclic RGD peptide. Ephrin-A1 and RGD were incubated in the molar ratios indicated above each panel and show EphA2 translocation regardless of the

area of the cell–supported membrane contact. (**E**) Mechanical reorganization of EphA2 requires a fluid membrane. Bilayers composed of 99.9% DPPC and 0.1% biotin-DPPE are not fluid during cell engagement at 37°C; as a result, no long-range EphA2 reorganization is observed on DPPC bilayers. (**F**) Western blots of lysates collected from 1×10^5 cells cultured onto fluid and nonfluid membranes. Presentation of fluid ephrin-A1 results in more rapid and complete EphA2 activation than presentation of nonfluid ephrin-A1, as measured by EphA2 degradation and total phosphorylated tyrosine intensities. EphA2 bands are at a mass of ~100 kD. (**G**) When cells were treated with the Rho kinase inhibitor Y-27632, a dosage-dependent decrease in Eph-ephrin radial transport was observed ($n = 627$ cells), demonstrating that the cytoskeleton drives radial transport. Experiments were performed in duplicate, and radial transport was independently normalized to untreated samples from each replicate. Error bars indicate SE for at least 139 cells at each dosage.

revealed progressively larger cell–supported membrane contact areas with increasing RGD peptide density, but with no change in EphA2 organization (Fig. 2D). Immunostaining for β_1, $\alpha_V\beta_3$, and $\alpha_V\beta_5$ integrins, known markers of focal adhesions, did not show colocalization with EphA2 (fig. S10). Thus, we conclude that the radial transport of EphA2 is selective and independent of integrin-mediated adhesion and signaling.

Importantly, radial transport of ligand-stimulated EphA2 is dependent on the lateral mobility of ephrin-A1 in the supported membrane. Fully saturated 1,2-dipalmitoyl-*sn*-glycero-3 phosphocholine (DPPC) lipids form a nonfluid bilayer in the gel phase at 37°C, and ephrin-A1 displayed on these membranes (22) failed to exhibit microcluster formation or inward transport upon interaction with cells (Fig. 2E). This correlated with differ-ences in EphA2 signaling as measured by receptor phosphorylation and degradation, which are hallmarks of ligand-induced activation (16). When identical numbers of cells (~1 × 10^5) were plated onto fluid and nonfluid supported membranes doped with an identical density of ephrin-A1 binding sites (1:1000 biotin-DPPE), the ephrin-A1 tethered to nonfluid DPPC membranes induced ~50% less EphA2 degradation and ~40% less tyrosine phosphorylation than did ephrin-A1 tethered to control fluid membranes (Fig. 2F). Furthermore, on fluid membranes, ephrin-A1 clusters colocalized with the areas of highest tyrosine phosphorylation, and radial transport of Eph-ephrin complexes coincided with substantial f-actin reorganization (Fig. 2C and fig. S11).

Cytoskeleton reorganization is known to result from ligand-dependent tyrosine phosphorylation of EphA2 and subsequent downstream signaling processes (29). This ultimately contributes to cell contact–dependent repulsion and tissue patterning (15). EphA2 can remodel the cytoskeleton through activation of the small guanosine triphosphatase RhoA (30), a process implicated in the high motility and invasive ability of malignant tumor cells (31). To explore the effects of this process on EphA2 transport, we used the selective Rho-associated kinase inhibitor Y-27632 to block actomyosin contractility (32). MDA-MB-231 cells treated with inhibitor concentrations ranging from 1 to 50 μM exhibited a dose-dependent decrease in their capacity to transport EphA2-ephrin-A1 complexes to the center of the cell–supported membrane contact junction (Fig. 2G). This observation indicates that EphA2 transport is actively driven by actomyosin contractile forces.
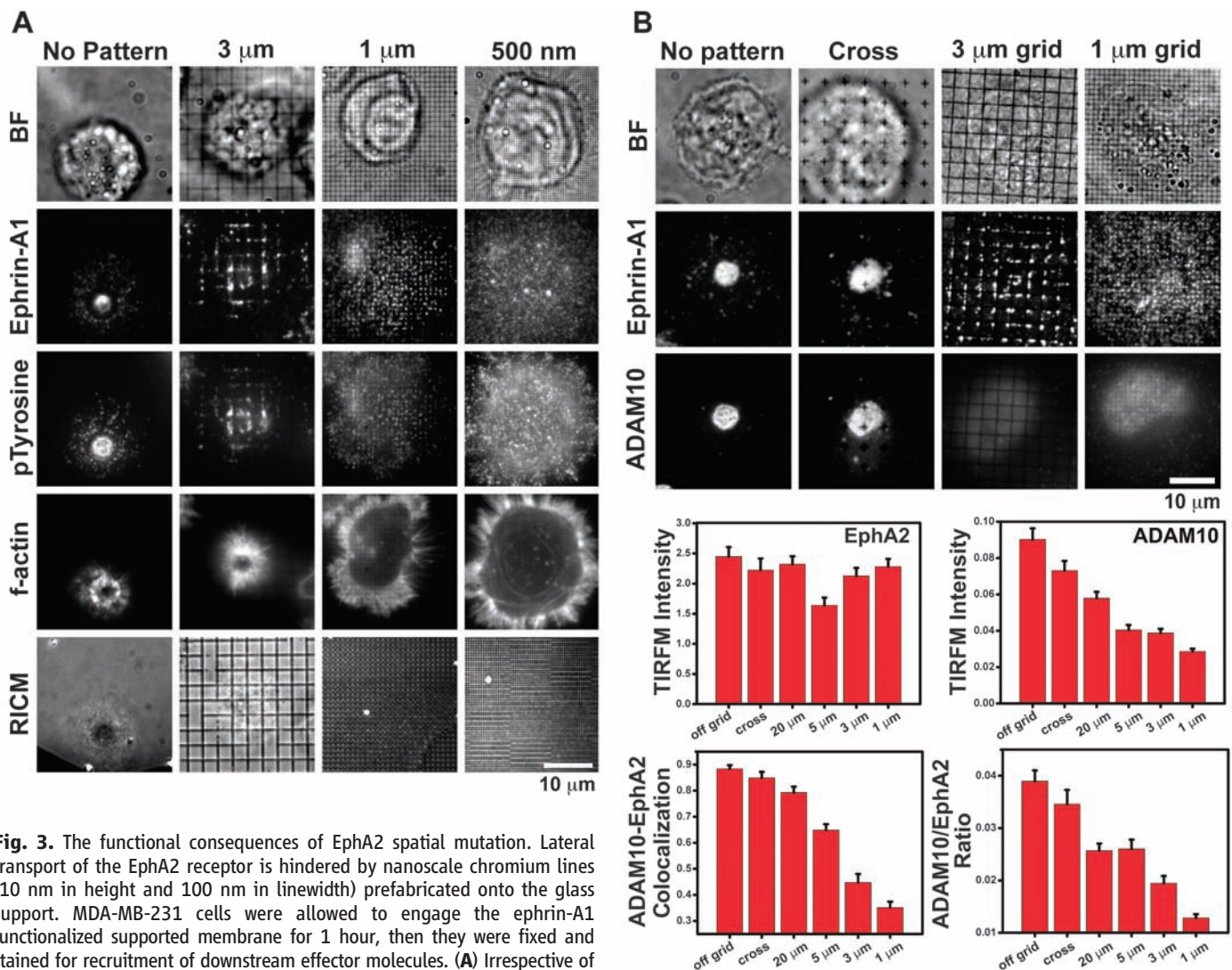

Fig. 3. The functional consequences of EphA2 spatial mutation. Lateral transport of the EphA2 receptor is hindered by nanoscale chromium lines (10 nm in height and 100 nm in linewidth) prefabricated onto the glass support. MDA-MB-231 cells were allowed to engage the ephrin-A1 functionalized supported membrane for 1 hour, then they were fixed and stained for recruitment of downstream effector molecules. (**A**) Irrespective of the presence or the scale of spatial mutations, phosphorylated tyrosine colocalized with ephrin-A1. F-actin adopted an annulus peripheral to the receptor-ligand assembly when EphA2 transport was unrestricted. However, when EphA2 organization was altered, the cytoskeleton assumed a spread morphology with f-actin primarily present in peripheral lamellipodia. The spread actin morphology switched to an annulus surrounding the EphA2-ephrin-A1 assembly when cells were exposed to 3-μm–pitch barriers. (**B**) ADAM10 colocalized with the EphA2-ephrin-A1 assembly on unrestricted supported membranes. However, when EphA2 transport was restricted by metal lines on the silica substrate, the measured colocalization decreased, and the ratio of ADAM10 to EphA2 also decreased (n = 477 cells). This indicates that mechanical restriction of EphA2 modulates ADAM10 recruitment.
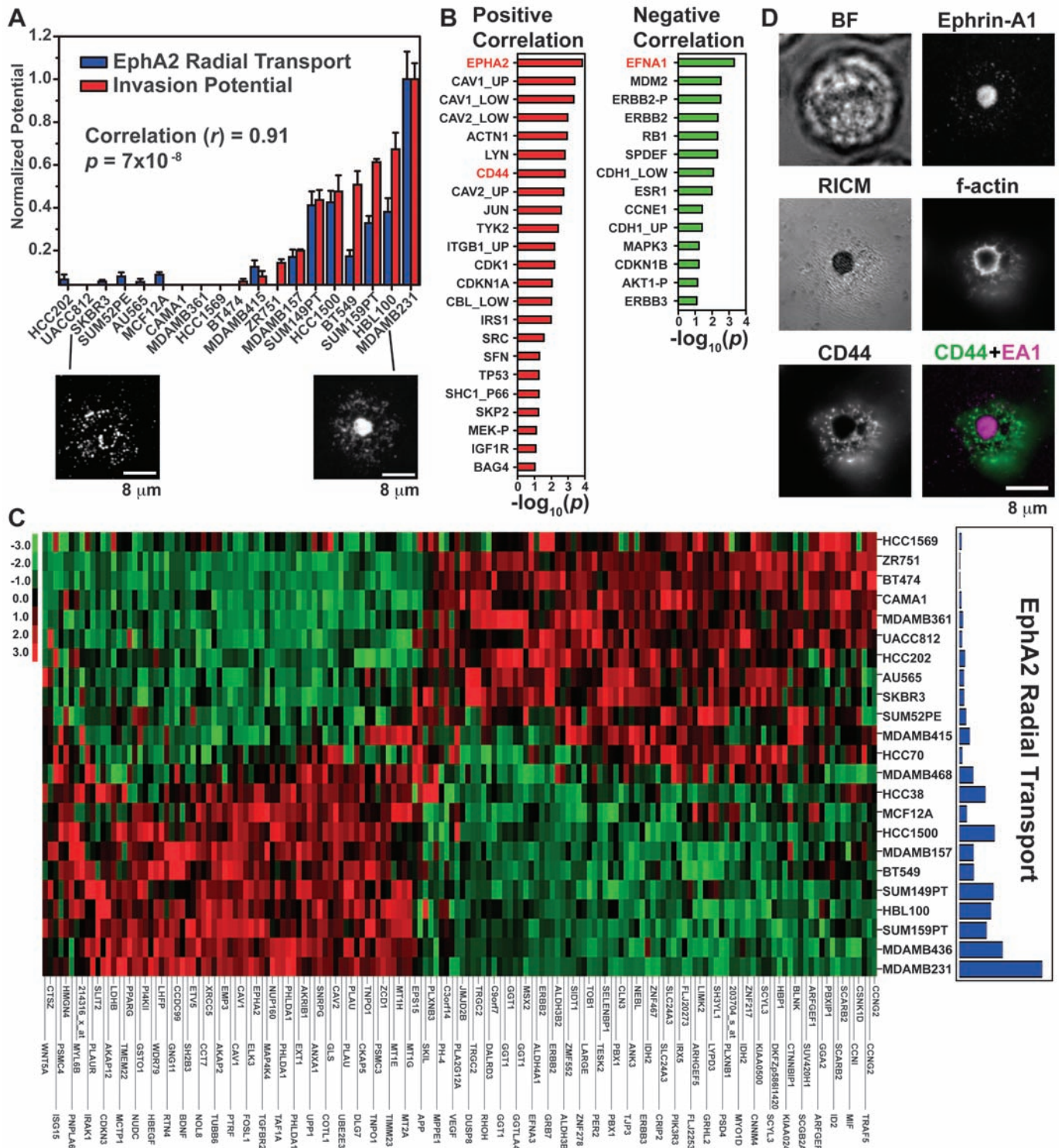
Fig. 4. Correlation of EphA2 radial transport to molecular and behavior properties in breast cancer. The average ephrin-A1 ligand radial distribution functions for 26 cell lines are quantified, parameterized, and then used as a spatial biomarker that is directly correlated to known biological characteristics and proteomic and genomic expression levels. (**A**) The average radial distribution function was found to exhibit a strong correlation ($r = 0.91$, $p = 7 \times 10^{-8}$) to invasion potentials that were determined with modified Boyden chamber analysis. (**B**) The proteomic correlates ($p < 0.1$) of EphA2 radial transport are shown in the table with their associated p values and are grouped based on the type of association (positive or negative). Proteins highlighted in red are those whose role in EphA2 reorganization has been experimentally observed. (**C**)

Transcriptomic correlates ($p < 1 \times 10^{-4}$, false discovery rate $< 5 \times 10^{-3}$) of EphA2 radial transport are illustrated in a heat map. Unsupervised hierarchical clustering of expression profiles of mRNAs that are predicted to be surrogates of EphA2 radial transport shows two distinct clusters of cell lines associated with the phenotype. Red indicates up-regulated expression, whereas green indicates down-regulated expression. (**D**) Representative bright field, epifluorescence immunostaining, and RICM images of a cell 1 hour after plating on a supported membrane functionalized with ephrin-A1. The cell adhesion molecule CD44 was found to be substantially up-regulated in protein expression in cells that underwent EphA2 radial transport. This signaling molecule was also found to be antilocalized with EphA2 upon ligand-induced activation.

To examine the functional consequences of EphA2 transport, we physically manipulated EphA2 spatial organization. Supported membranes were formed on glass substrates with various patterns of metal lines (100-nm line-width and 10-nm height) prefabricated by electron beam lithography (22). These create barriers to lateral transport within the supported membrane without otherwise influencing mobility or altering topography (fig. S12). Lipids and membrane-tethered proteins diffuse freely but cannot cross barriers (fig. S13) (7, 10, 33). Upon binding its supported membrane–bound ephrin-A1 ligand, the EphA2 receptor and other physically associated signaling molecules become subject to the same geometrical constraints to mobility. The approach applies physical perturbations to the living cell exclusively through specific receptor-ligand couplings, and the entire ensemble of receptors is uniformly affected. A variety of non-native EphA2 spatial configurations were generated by engaging cells with patterned membranes whose grid pitches ranged from 0.5 to 20 μm (Fig. 3). Immunofluorescence imaging of cells on grid-patterned constraints reveals that the confined EphA2 clusters remain heavily phosphorylated in all cases (unrestricted, 3-, 1-, and 0.5-μm–pitch barriers). EphA2 is locally triggered irrespective of geometrical constraint (Fig. 3A).

In contrast, the morphology of the f-actin exhibited two discrete states as a function of the degree of physical partitioning forced onto the EphA2 receptor pattern. Cells engaging membranes with 500-nm–pitch barriers displayed a spreading morphology, with f-actin primarily in peripheral lamellipodia. This behavior is similar to that observed in cells cultured on standard glass slides or on RGD-functionalized surfaces without ephrin (fig. S14). The actin morphology dramatically changed into an annulus immediately surrounding the EphA2-ephrin-A1 assembly when cells were exposed to substrates with grid barrier pitches of 3 μm or larger (Fig. 3A). These observed differences in f-actin morphology at identical ephrin-A1 densities indicate that physical resistance to EphA2 receptor transport can change the threshold for ephrin-A1–triggered cytoskeleton reorganization.

The recruitment of effector molecules such as phosphatases or proteases is one mechanism used to dampen EphA2 signaling levels. In particular, ADAM10, a zinc-dependent transmembrane protease, is implicated in the ectodomain trans-shedding of ephrin-As as a consequence of Eph receptor binding (17). ADAM10 has been shown to weakly associate with Eph receptors at the plasma membrane and to preferentially bind receptor-ligand complexes. Proteolytic cleavage by ADAM10 occurs at the extracellular domain of ephrin-As and is hypothesized to initiate release and endocytosis of the receptor-ligand complex (17). Disengagement of the physical tether between apposed cells is thought to play a role in the observed Eph-driven cell repulsion, rather

than the cell adhesion that might be anticipated due to strong receptor-ligand binding (14, 17). When cells were triggered with fluid ephrin-A1 for 1 hour and stained for ADAM10, we observed that ADAM10 was selectively recruited to the cell–supported membrane interface (Fig. 3B and figs. S5 and S15). However, when the EphA2 radial transport was mechanically hindered with metal grid patterns, ADAM10 recruitment was substantially reduced, and selective colocalization with EphA2 was abrogated at the 60-min time point (Fig. 3B). Cross-shaped metal patterns with a similar coverage area to that of the grids (4% of surface area) still allow ephrin-A1 radial transport and do not drastically affect ADAM10 recruitment. This confirms that ADAM10 recruitment can be regulated by physically interfering with EphA2 transport and is not simply diminished by the presence of metal patterns in the supported membrane.

To quantify ADAM10 recruitment to receptor-ligand complexes, TIRFM was used to measure cell surface EphA2 and ADAM10 levels of an identical set of cells ($n = 477$ cells) that displayed a range of receptor spatial mutations. Whereas the amount of EphA2 remained constant, the amount of recruited ADAM10 decreased with the size of the observed EphA2-ephrin-A1 clusters (Fig. 3B). In addition, the colocalization of ADAM10 with EphA2 (as measured by Pearson correlation coefficient r) also decreased. Control experiments with cross-shaped metal lines and 20-μm–pitch grids all confirm that these results are a consequence of receptor spatial organization and physical constraint. Cells cultured on two-component membranes displaying the cyclic RGD peptide along with ephrin-A1 displayed the same response to spatial mutations, confirming that this phenomenon is independent from RGD-mediated integrin adhesion and signaling (fig. S16).

These spatial mutation experiments demonstrate that physical manipulation of EphA2–ephrin-A1 microcluster organization alters the cellular response to ephrin-A1. There are both spatial and mechanical aspects to these results. The cell applies force, via actomyosin contractility, to ligand-engaged EphA2 receptors. According to Newton's third law, grid barriers that block EphA2 transport in the spatial mutation must necessarily exert opposing forces on the receptor clusters. Spatial organization and mechanical forces are thus interconnected, resulting in an overall sensitivity of the EphA2 signaling pathway to spatio-mechanical aspects of the cellular microenvironment in which ephrin-A1 is displayed.

To investigate the generality of ligand-induced EphA2 transport beyond the MDA-MB-231 cell line, we examined a library of breast cancer cell lines. Such cell lines derived from primary tumors have been the most widely used models to elucidate how genes and signaling pathways regulate disease progression (34). When a panel of cell lines is used as a system, rather than individually, it can serve as a powerful tool to identify

and investigate recurrent markers for disease progression (35). Therefore, the propensity to radially transport the EphA2 receptor was characterized in 26 cell lines (22, 34). An aliquot of ~50×10^3 cells was plated onto ephrin-A1–functionalized supported membranes for 1 hour for each cell line. Live-cell fluorescence microscopy was used to image the resulting distribution of ligand under individual cells, and a signature radial distribution function was determined for each cell line type. Radial transport was not unique to MDA-MB-231; rather, each cell line tested displayed a distinct and characteristic degree of ligand-induced receptor reorganization (fig. S17). The diversity observed in EphA2 transport between different cell lines may result from the wide range of deregulations inherent to this library, as well as variance in EphA2 expression levels. To quantify the EphA2 radial transport phenotype, we parameterized the radial distribution functions for each cell line using linear regression, integration of area under the curve, and the ratio of peak-height to peak-width at half-maximum at time $t = 60$ min (fig. S18). These different scoring methods were robust and led to very similar values across the cell-line library.

To identify the molecular signature of this spatial organization phenotype, we next performed large-scale analyses using the wealth of available data for the panel of cell lines (22). In these analyses, the measured radial transport scores serve as an unconventional spatial biomarker unique to each cell line and potentially associated with genomic, proteomic, or phenotypic signatures in neoplasia. Invasion potentials, as measured using a modified Boyden chamber assay (34), were strongly linked (Pearson correlation $r = 0.91$, $p = 7 \times 10^{-8}$) to the receptor radial transport phenotype across the library (Fig. 4A). In contrast, EphA2 mRNA and protein expression levels did not correlate as strongly with invasion potentials, and the correlation values (r) were 0.64 and 0.53, respectively, in agreement with previous reports (34, 36). EphA2 translocation is distinct from expression, and a stronger degree of association is found between the scored receptor radial transport phenotype and invasion potentials across the breast cancer model, suggesting a link between EphA2 radial transport and tissue invasion. Additionally, a system-wide correlation of the spatial organization scores to protein and mRNA expression levels revealed 37 proteins ($p < 0.1$) and 141 mRNA transcripts ($p < 1 \times 10^{-4}$, 158 probe sets) that are associated with this phenotype (Fig. 4, B and C, and tables S1 and S2). Searches of the Kyoto Encyclopedia of Genes and Genomes and BioCarta pathway analysis databases (37) revealed that radial transport was associated with the ErbB, p53, integrin, and MAPK signaling pathways (tables S3 and S4). Notably, all of these pathways have been previously reported to associate with invasiveness and EphA2 signaling; we now show that they also associate with EphA2 spatial organization (36).

One of the proteins identified through this screen was CD44, a cell membrane-bound glycoprotein involved in cell adhesion and migration (*38*). The spatial organization of CD44 upon ephrin-A1 stimulation was found to antilocalize with the assembly of EphA2 (Fig. 4D), validating the involvement of CD44 in cell-driven EphA2 receptor reorganization. The system-wide correlation analysis does not necessarily provide the mechanistic details leading to EphA2 sorting; instead, it identifies proteins and genes that may serve as surrogate markers to centripetal transport.

In conclusion, we report a spatio-mechanical regulation of the EphA2 signaling pathway. Upon membrane-bound ligand stimulation, EphA2 is transported radially inwards by an actomyosin contractile process. Physical interference with this transport, which necessarily involves the imposition of opposing forces on EphA2, alters ligand-induced EphA2 activation as observed by the recruitment of the protease ADAM10 and cytoskeleton morphology. Quantitative measurement of centripetal receptor transport across a library of mammary epithelial cell lines reveals a high correlation with invasion potential and with specific gene and protein expression. These observations suggest that spatio-mechanical aspects of ephrin-A1 expressing cells and their surrounding tissue environment may functionally alter the response of EphA2 signaling systems and could play a contributing role in the onset and progression of cancer.

References and Notes

1. D. E. Discher, P. Janmey, Y.-l. Wang, *Science* **310**, 1139 (2005).
2. M. J. Dalby *et al.*, *Nat. Mater.* **6**, 997 (2007).
3. C. M. Nelson, M. M. VanDuijn, J. L. Inman, D. A. Fletcher, M. J. Bissell, *Science* **314**, 298 (2006).
4. D. T. Butcher, T. Alliston, V. M. Weaver, *Nat. Rev. Cancer* **9**, 108 (2009).
5. C. S. Chen, *J. Cell Sci.* **121**, 3285 (2008).
6. S. Y. Qi, J. T. Groves, A. K. Chakraborty, *Proc. Natl. Acad. Sci. U.S.A.* **98**, 6548 (2001).
7. K. D. Mossman, G. Campi, J. T. Groves, M. L. Dustin, *Science* **310**, 1191 (2005).
8. N. L. Andrews *et al.*, *Nat. Cell Biol.* **10**, 955 (2008).
9. S. Hurtley, *Science* **326**, 1205 (2009).
10. N. C. Hartman, J. A. Nye, J. T. Groves, *Proc. Natl. Acad. Sci. U.S.A.* **106**, 12729 (2009).
11. J. D. Scott, T. Pawson, *Science* **326**, 1220 (2009).
12. R. O. Hynes, *Science* **326**, 1216 (2009).
13. T. Marquardt *et al.*, *Cell* **121**, 127 (2005).
14. M. Lackmann, A. W. Boyd, *Sci. Signal.* **1**, re2 (2008).
15. K. Kullander, R. Klein, *Nat. Rev. Mol. Cell Biol.* **3**, 475 (2002).
16. J. Walker-Daniels, D. J. Riese II, M. S. Kinch, *Mol. Cancer Res.* **1**, 79 (2002).
17. P. W. Janes *et al.*, *Cell* **123**, 291 (2005).
18. S. Davis *et al.*, *Science* **266**, 816 (1994).
19. J. T. Groves, *Curr. Opin. Chem. Biol.* **10**, 544 (2006).
20. J. T. Groves, N. Ulman, S. G. Boxer, *Science* **275**, 651 (1997).
21. J. M. Nam, P. M. Nair, R. M. Neve, J. W. Gray, J. T. Groves, *ChemBioChem* **7**, 436 (2006).
22. Materials and methods are available as supporting material on *Science* Online.
23. W. J. Galush, J. A. Nye, J. T. Groves, *Biophys. J.* **95**, 2512 (2008).
24. J.-P. Himanen *et al.*, *Nature* **414**, 933 (2001).
25. B. Day *et al.*, *J. Biol. Chem.* **280**, 26526 (2005).
26. J. P. Himanen *et al.*, *Nat. Neurosci.* **7**, 501 (2004).
27. H. Verschueren, *J. Cell Sci.* **75**, 279 (1985).
28. J. D. Humphries, A. Byron, M. J. Humphries, *J. Cell Sci.* **119**, 3901 (2006).
29. N. Carter, T. Nakamoto, H. Hirai, T. Hunter, *Nat. Cell Biol.* **4**, 565 (2002).
30. M. L. Taddei *et al.*, *Am. J. Pathol.* **174**, 1492 (2009).
31. P. Friedl, K. Wolf, *Nat. Rev. Cancer* **3**, 362 (2003).
32. P. P. Provenzano, D. R. Inman, K. W. Eliceiri, S. M. Trier, P. J. Keely, *Biophys. J.* **95**, 5374 (2008).
33. J. T. Groves, S. G. Boxer, *Acc. Chem. Res.* **35**, 149 (2002).
34. R. M. Neve *et al.*, *Cancer Cell* **10**, 515 (2006).
35. T. Vargo-Gogola, J. M. Rosen, *Nat. Rev. Cancer* **7**, 659 (2007).
36. M. Macrae *et al.*, *Cancer Cell* **8**, 111 (2005).
37. G. Dennis Jr. *et al.*, *Genome Biol.* **4**, P3 (2003).
38. H. Ponta, L. Sherman, P. A. Herrlich, *Nat. Rev. Mol. Cell Biol.* **4**, 33 (2003).
39. We thank N. Bayani for assistance in performing Western blotting, A. Smoligovets and C.-H. Yu for performing transfection and imaging with EGFP-actin–expressing MDA-MB-231 cells, and A. Bershadsky for helpful discussions. This work was supported by the Director, Office of Science, Office of Basic Energy Sciences, Chemical Sciences, Geosciences, and Biosciences Division (K.S.; P.M.N.; hybrid synthetic-live cell interfaces) and the Materials Sciences and Engineering Division (R.S.P.; supported membrane substrates) of the U.S. Department of Energy (DOE) under contract no. DE-AC02-05CH11231. Patterned substrate fabrication was performed, in part, at the Molecular Foundry, Lawrence Berkeley National Laboratory (LBNL), and was supported by the Office of Science, Office of Basic Energy Sciences, Scientific User Facilities Division, of the U.S. DOE under contract no. DE-AC02-05CH11231. This work was also supported by the Laboratory Directed Research and Development Program of LBNL under U.S. DOE contract no. DE-AC02-05CH11231. Seed support for biomedical aspects of this work was provided by the U.S. Department of Defense Breast Cancer Research Program Concept Award BC076701 under U.S. Army Medical Research Acquisition Activity no. W81XWH-08-1-0677, with follow-on support provided by Award U54 CA143836 from the National Cancer Institute (NCI) beginning in 2009. The content is solely the responsibility of the authors and does not necessarily represent the official views of the NCI or the NIH. J.W.G. acknowledges support from the Director, Office of Science, Office of Biological and Environmental Research, of the DOE under conract no. DE-AC02-05CH11231; the NIH; NCI grant P50 CA 58207; and the NIH NCI Integrative Cancer Biology Program grant number U54 CA 112970 to J.W.G. (bioinformatics and cell lines). The Regents of the University of California have filed a related patent application through LBNL.

Lgr6 Marks Stem Cells in the Hair Follicle That Generate All Cell Lineages of the Skin

Hugo J. Snippert,[1]* Andrea Haegebarth,[1]* Maria Kasper,[2] Viljar Jaks,[2] Johan H. van Es,[1] Nick Barker,[1] Marc van de Wetering,[1] Maaike van den Born,[1] Harry Begthel,[1] Robert G. Vries,[1] Daniel E. Stange,[1] Rune Toftgård,[2] Hans Clevers[1]†

Mammalian epidermis consists of three self-renewing compartments: the hair follicle, the sebaceous gland, and the interfollicular epidermis. We generated knock-in alleles of murine *Lgr6*, a close relative of the *Lgr5* stem cell gene. *Lgr6* was expressed in the earliest embryonic hair placodes. In adult hair follicles, Lgr6+ cells resided in a previously uncharacterized region directly above the follicle bulge. They expressed none of the known bulge stem cell markers. Prenatal Lgr6+ cells established the hair follicle, sebaceous gland, and interfollicular epidermis. Postnatally, Lgr6+ cells generated sebaceous gland and interfollicular epidermis, whereas contribution to hair lineages gradually diminished with age. Adult Lgr6+ cells executed long-term wound repair, including the formation of new hair follicles. We conclude that Lgr6 marks the most primitive epidermal stem cell.

In the adult skin, interfollicular epidermis (IFE) and sebaceous glands (SGs) are subject to constant self-renewal, whereas hair follicles (HFs) cycle between growth, involution, and resting phases (fig. S1) (*1*). Under normal conditions, these three skin cell populations are each believed to be maintained by their own discrete stem cells (*2*). When tissue homeostasis is disrupted, however, any of the three stem cell populations is capable of producing all three structures (*2*, *3*). The IFE can be maintained without the recruitment of stem cells from the HF bulge (*4*–*8*), yet the exact identification of IFE stem cells has remained elusive. Within the SG, progenitors reportedly maintain this structure independent of the HF (*5*, *9*). HF stem cells

[1]Hubrecht Institute–KNAW (Royal Netherlands Academy of Arts and Sciences) and University Medical Center Utrecht, Uppsalaalaan 8, 3584 CT Utrecht, Netherlands. [2]Karolinska Institutet, Center for Biosciences and Department of Biosciences and Nutrition, Novum, SE-141 57 Huddinge, Sweden.

*These authors contributed equally to this work.
†To whom correspondence should be addressed. E-mail: h.clevers@hubrecht.eu